Methods 59 (2013) 278–286

Contents lists available at SciVerse ScienceDirect

Methods

journal homepage: www.elsevier.com/locate/ymeth

Review Article

Investigations of protein–protein interactions using time-resolved fluorescence and phasors

David M. Jameson *, Carissa M. Vetromile, Nicholas G. James

University of Hawaii, Department of Cell and Molecular Biology, John A. Burns School of Medicine, 651 Ilalo St., BSB222, Honolulu, HI 96813, USA

ARTICLE INFO

Article history:
Available online 22 January 2013

Communicated by Peter Schuck

ABSTRACT

Protein interactions are critical for biological specificity and techniques able to characterize these interactions are of fundamental importance in biochemistry and cell biology. Fluorescence methodologies have been extremely useful for studying many biological systems including protein–ligand and protein–protein interactions. In this review we focus on the application of time-resolved fluorescence approaches to macromolecular systems. We also include a detailed discussion of a relatively new time-resolved technique, the phasor method, for studying protein interactions both *in vitro* and in live cells.

1. Introduction

Protein–protein interactions underlie most biological processes and the development of methods to identify such interactions and to elucidate their strength and specificity is an active area of research. Many such methods are based on hydrodynamic properties of proteins and protein complexes. For example, ultra centrifugation and size-exclusion chromatography can be used to estimate the size of protein complexes and to provide information on the stoichiometry and affinity of the binding partners. Since the pioneering work of Gregorio Weber [1], fluorescence methodologies, including polarization and time-resolved approaches, have been successfully used to investigate macromolecular interactions. In this review we shall focus on time-resolved approaches to this area, including time-decay anisotropy. We shall also discuss the application of the more recent phasor approach in this area. We shall first describe time-resolved fluorescence methods in general, and we shall introduce the phasor approach, in particular its application to *in vitro* studies. We shall then discuss time-decay anisotropy and dynamic polarization. Then we shall review the application of phasors to fluorescence lifetime imaging microscopy (FLIM), especially to Förster resonance energy transfer (FRET) studies.

2. Time-resolved fluorescence and phasors

The application of fluorescence methodologies to the study of protein–protein interactions first requires identification of an appropriate fluorophore. In some cases, the protein's intrinsic tryptophan fluorescence may be utilized [2] or there may be an intrinsic fluorescence cofactor, such as NADH, FAD, or a fluorescent porphyrin associated with one or both of the proteins. Alternatively, an extrinsic fluorophore may be introduced into the system, usually by covalent labeling with an amine or cysteine-reactive probe. "The Molecular Probes® Handbook-A Guide to Fluorescent Probes and Labeling Technologies", specifically the 11th edition, is a comprehensive and thorough source for information on the chemistries of probe-protein labeling. The chemistry of protein reactive groups and diverse labeling reagents used for protein conjugation are discussed in the general literature and in texts [3,4]. If the objective is to study protein associations in living cells then introduction of fluorophores usually requires the use of molecular biological approaches [5]. Once a suitable fluorophore is introduced, the fluorescence methodology must be selected. In some cases, steady-state polarization/anisotropy approaches may be appropriate: for a recent review of these techniques see [6]. In the present review, however, we shall focus on time-resolved methodologies.

Time-resolved fluorescence data are typically obtained using either frequency- or time-domain methodologies. In the time-domain, the excitation source delivers a pulse of light which, ideally, is very short compared to the fluorescence lifetime [7]. Typically, mode-locked lasers or, more recently, pulsed light emitting diodes (LEDs) have been utilized [8]. Modern laser sources can deliver pulses of picosecond duration or less. In the frequency domain approach, the intensity of the exciting light is typically modulated sinusoidally at variable frequencies, usually in the megahertz range. This light modulation was historically achieved using devices such as the Kerr cell [9], the Debye-Sears tank [10], or the Pockels cell [11]. In recent years, light sources such as laser diodes (LD) or light emitting diodes (LEDs) with directly modulated

* Corresponding author.
E-mail address: djameson@hawaii.edu (D.M. Jameson).

1046-2023/$ - see front matter © 2013 Elsevier Inc. All rights reserved.
http://dx.doi.org/10.1016/j.ymeth.2013.01.004

outputs have been utilized for frequency domain fluorescence lifetime determinations [12]. In addition to sinusoidal modulation, repetitive light sources, such as synchrotron radiation and mode-locked lasers have also been used for frequency-domain measurements by utilizing the harmonic content of the pulse train [13,14].

The traditional approaches to time-resolved fluorescence analysis fit the time dependent fluorescence intensity decay data to various models, such as multi-exponential decays or distributions [2,15,16]. The maximum entropy method has also been used to treat lifetime data [17]. In the case of frequency-domain measurements, the data are typically in the form of phase angles and modulation ratios, as illustrated in Fig. 1.

It was demonstrated as early as 1933 [18] that tan $\phi = \tau_P \omega$ (where ϕ represents the phase delay between the excitation and emission, and ω is the angular modulation frequency, which is equal to $2\pi f$ where f is the linear modulation frequency) and hence the phase delay gives one measure of the excited state lifetime, τ_P. The so-called modulations of the excitation (M_E) and the emission (M_F) are given by:

$$M_E = \left(\frac{AC}{DC}\right)_E \quad \text{and} \quad M_F = \left(\frac{AC}{DC}\right)_F \tag{1}$$

where the terms AC and DC refer to the alternating signal (AC) and the average signal (DC) as indicated in Fig. 1. Then the relative modulation (also known as the modulation ratio), M, of the emission, which is the ratio of the modulations of the exciting light and the emission [18], is given by:

$$M = \frac{(AC/DC)_F}{(AC/DC)_E} \tag{2}$$

The excited state lifetime, τ_m, can also be determined from M according to the relation

$$M = \frac{1}{\sqrt{1 + (\omega\tau_m)^2}} \tag{3}$$

Readers interested in the derivation of these equations may refer to the seminal paper by Spencer and Weber [10]. Hence, by measuring the phase shift and modulation ratio one can determine a phase lifetime (τ_P) and a modulation lifetime (τ_M). If the fluorescence decay is a single exponential, then τ_P and τ_M will be equal at all

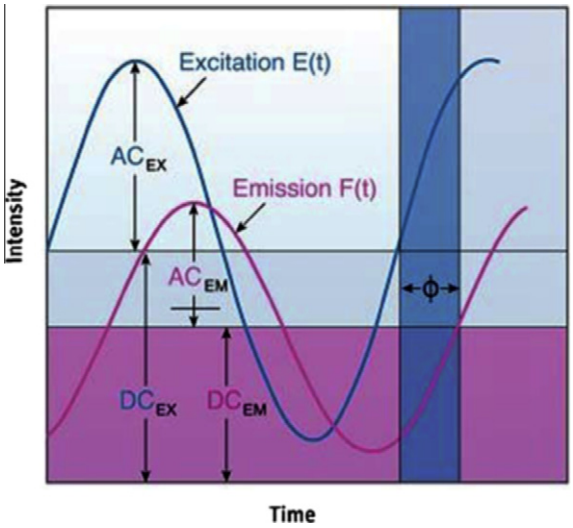

Fig. 1. Sketch depicting excitation (blue) and emission (red) waveforms corresponding to frequency domain phase and modulation measurements. The phase delay (Φ) between the excitation and emission is illustrated along with the AC and DC components of each waveform.

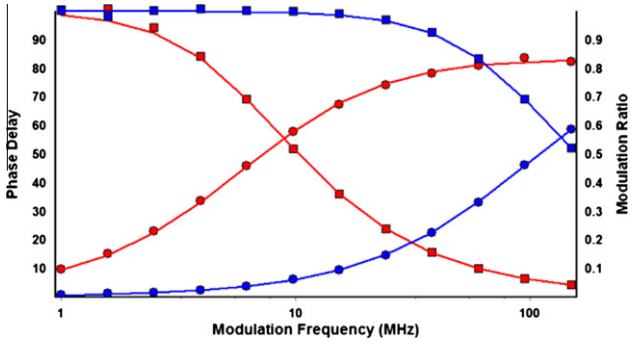

Fig. 2. Phase (circles) and modulation (squares) data corresponding to ethidium bromide free in solution (blue) and bound to transfer RNA (red).

modulation frequencies. However, if the fluorescence decay is multiexponential then $\tau_P < \tau_M$ and, moreover, the values of both τ_P and τ_M will depend upon the modulation frequency, specifically, both the phase and modulation lifetimes will decrease as the excitation light modulation frequency increases. These differences between τ_P and τ_M, and their frequency dependence, form the basis of the methods used to analyze lifetime heterogeneity, i.e., the component lifetimes and amplitudes. Frequency domain, i.e., phase and modulation data, are typically displayed as shown in Fig. 2. In the case shown, namely ethidium bromide (EB) in aqueous buffer and in the presence of an excess of transfer RNA, both data sets can be well-fit to a single exponential decay; 1.74 and 27 ns for free and bound EB, respectively. These data can also be viewed using the phasor approach discussed below. In 1981, Weber defined two terms S and G as: $S = M \sin\theta$ and $G = M \cos\theta$, where M and θ are the modulation ratio and phase angle of the emission, respectively [19]. Weber also demonstrated that the S and G functions could be derived from time domain data according to the equations:

$$\begin{aligned} G(\omega) &= \int_0^\infty I(t)\cos(\omega t)dt \Big/ \int_0^\infty I(t)dt \\ S(\omega) &= \int_0^\infty I(t)\sin(\omega t)dt \Big/ \int_0^\infty I(t)dt \end{aligned} \tag{4}$$

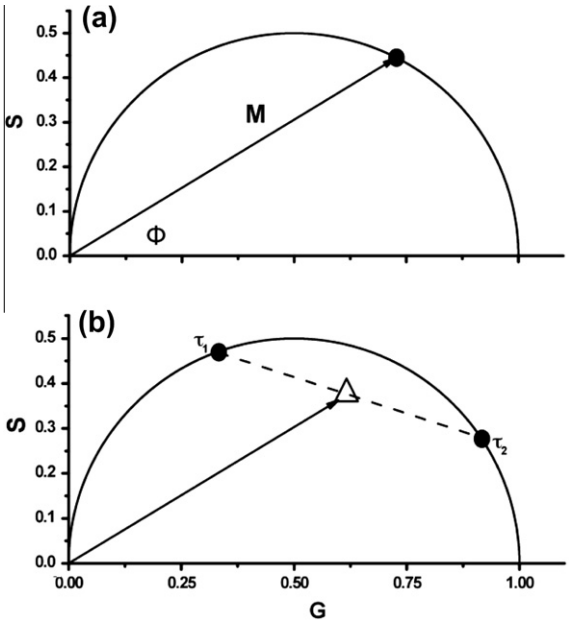

Fig. 3. Phasor plots corresponding to a single exponential decay (a) and a system containing two discrete lifetime components (b).

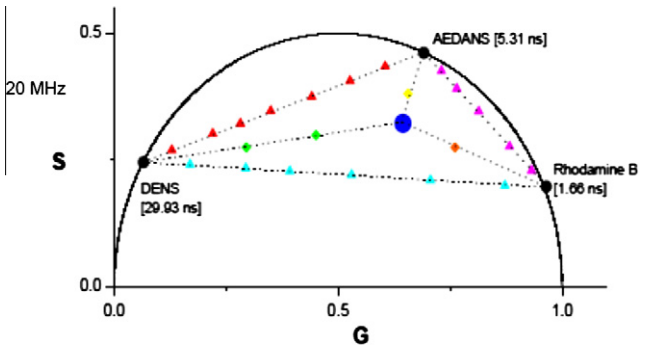

Fig. 4. Phasor plots taken at 20 MHz light modulation frequency for three different fluorophores and for different mixtures of these fluorophores. One notes that binary mixtures give rise to phasor points along the line connecting the pure fluorophores while ternary mixtures result in phasor points inside the triangle formed by the three two component mixtures.

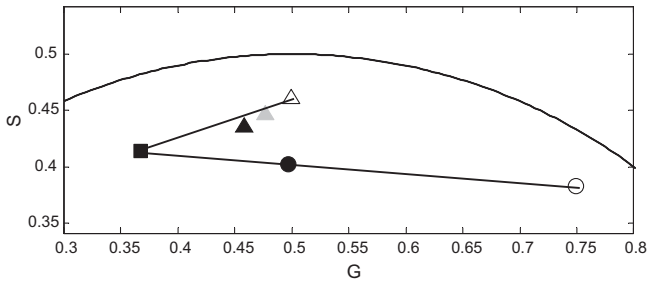

Fig. 5. Protein–protein interaction characterized by the phasor analysis. The projected linear movement (predicted for non-interacting molecules) of the phasor point between antithrombin (black square) plus lysozyme (open circle) or antithrombin plus thrombin (open triangle) is shown as a black line. The phasor point of the mixture of 1 μM antithrombin and 1 μM lysozyme follows the predicted path (filled circles; no interaction). However, increasing concentrations of antithrombin to a solution of 1 μM thrombin causes the phasor points to move in a non-linear path (filled triangles). This deviation denotes interaction among the two proteins as the lifetimes have been modified. Measurements were done at 20 °C with excitation at 280 nm with 43 MHz frequency.

where $I(t)$ is the intensity at time t and the angular modulation frequency, ω, can be the repetition rate of the pulsed light source or another value that is convenient to observe the kinetic process under investigation, in other words, one can choose a frequency that is one roughly on the same time scale as the lifetimes being observed. Jameson et al. [15] used these S and G values, to construct a phasor plot. At that time it was applied exclusively to frequency-domain data. This geometrical representation of the phase delay and modulation ratio is illustrated in Fig. 3. As shown in Fig. 3A, a single exponential decay will result in the S, G point on the so-called universal circle. As shown in Fig. 3B, if two different single exponential decays are plotted, any value resulting from a mixture of these components will fall along the line joining the points on the universal circle. A demonstration of this property was shown by Stefl et al. [20] using a mixture of three fluorophores, as reproduced in Fig. 4. As the light modulation frequency changes, the positions of the phasor points move in a predictable manner [20]. The useful properties of the phasor plot are discussed in this article for both *in vitro* and *in vivo* experiments.

The phasor approach was first utilized to correct frequency domain data for background contributions; a detailed description of this process is beyond the scope of this review but interested readers are referred to the original work [21]. In 1993, Hirschfeld et al. [22] independently introduced an approach, completely analogous to the aforementioned phasor approach, to evaluate ligand binding, specifically they studied the binding of calcium ions to calcium binding probes such as Quin-2 and Calcium Green; details of their approach can be found in their article.

The phasor approach was dormant for several years until several researchers began to apply it to FLIM, in particular the laboratories of Tom Jovin, Quentin Hanley, Andrew Clayton, Robert Clegg, and Enrico Gratton contributed to the development of the method (although the plots were called by different names, depending on the laboratory, e.g., phasor plots [23], AB plots [24] and polar plots [25]).

In 2011, we began to apply the phasor method to cuvette studies [20] and in particular to protein [26] and then nucleic acid [27] systems. We noted that phasor plots can be used to study proteins containing multiple tryptophan residues, i.e., systems which could prove to be intractable to traditional analysis approaches. Specifically, as shown in Fig. 5, proteins which do not interact (in this case lysozyme and antithrombin) will each give a characteristic phasor point (at a given light modulation frequency) and when mixed the resultant phasor point must lie along the line connecting the two original phasor points. The exact position of this mixture phasor point will depend upon the relative concentrations of the two proteins, and their relative quantum yields and extinction coefficients

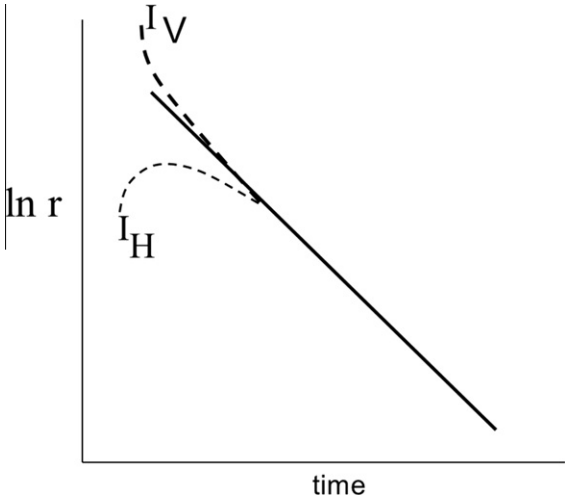

Fig. 6. Depiction of time-decay anisotropy data. The dotted lines correspond to the intensity decay of the vertical (I_V) and horizontal (I_H) polarized emission components while the solid line corresponds to the log of the anisotropy (lnr).

at the excitation wavelengths, as well as their respective lifetime components. If two proteins can interact, however, (in this case thrombin and antithrombin) then it is likely that the tryptophan emission of one or both proteins will be perturbed and the resulting phasor points will lie off of the line connecting the individual phasor points (Fig. 5). Hence, this approach can be used with intrinsic protein emission or with extrinsically labeled proteins, especially if the label exhibits some environmental sensitivity, e.g., acrylodan, and hence is likely to change its lifetime properties upon protein interaction.

3. Time-decay anisotropy and dynamic polarization

The technique of time-decay anisotropy, and its frequency domain equivalent of dynamic polarization, has been used for many years to extract information on the rotational modalities of macromolecules [7,28,29]. Although steady-state polarization/anisotropy methods provide information on the totality of the rotational processes of a system, it cannot quantitatively separate out individual contributions, for example from a mixture of components. In the

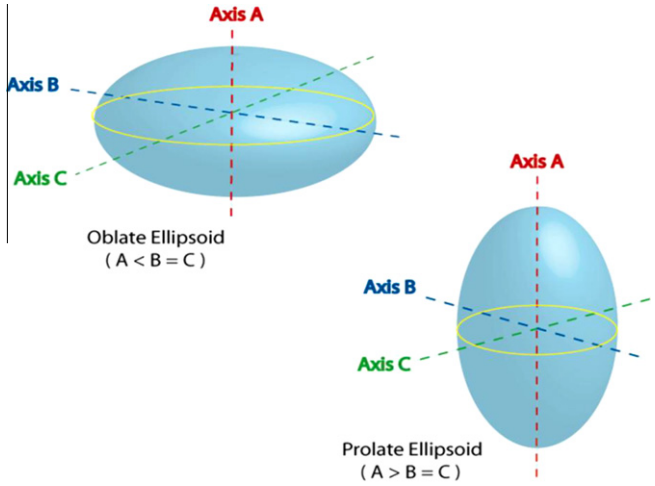

Fig. 7. Depiction of the principle rotational axes of prolate and oblate ellipsoids of revolution.

time-domain anisotropy method the sample is illuminated by a pulse of vertically polarized light and the decay over time of both the vertical and horizontal components of the emission are recorded. The anisotropy function is then plotted versus time as illustrated in Fig. 6. One notes that the horizontal component actually increases during short times, since initially the fluorophores have not rotated significantly. As time passes though, the number of horizontally oriented molecules increases.

The decay of the anisotropy with time, $r(t)$, for a sphere is given by:

$$r = \frac{Iv - Ih}{Iv + 2Ih} = r_o e^{-(t/\tau_c)} \tag{5}$$

where τ_c is the rotational correlation time, which in turn is related to the rotational diffusion coefficient by:

$$\tau_c = \frac{1}{6 \cdot D_{\text{rotation}}} \tag{6}$$

Interestingly, the rotational correlation time is exactly 1/3 the Debye rotational relaxation time, usually designated as ρ. The relationship between the rotational relaxation time for a sphere (ρ_o) and the molar volume of the rotating unit is given by:

$$\rho_o = \frac{3\eta V}{RT} \tag{7}$$

In the case of non-spherical particles, such as oblate or prolate ellipsoids (Fig. 7) the time-decay of anisotropy function is more complicated. Mathematically simple symmetrical ellipsoids give us a sense of how changes in shape affect the rotational diffusion rates.

In the case of symmetrical ellipsoids of revolution the relevant expression is [29]:

$$r(t) = r_1 e^{\left(\frac{-t}{\tau_{c1}}\right)} + r_2 e^{\left(\frac{-t}{\tau_{c2}}\right)} + r_3 e^{\left(\frac{-t}{\tau_{c3}}\right)} \tag{8}$$

where:

$$\begin{aligned} \tau_{c1} &= 1/6D_2 \\ \tau_{c2} &= 1/(5D_2 + D_1) \\ \tau_{c3} &= 1/(2D_2 + 4D_1) \end{aligned} \tag{9}$$

D_1 and D_2 are the rotational diffusion coefficients about the axes of symmetry and about either equatorial axis, respectively. Resolution of the rotational rates is limited in practice to two rotational correlation times which differ by at least a factor of two. The anisotropy amplitudes (r_1, r_2, and r_3) are complex functions related to the orientation of the emission dipole of the fluorophore along the various rotational axes of the rotating molecule, as shown if Fig. 8 (we assume here that the excitation and emission dipoles are colinear), specifically [29]:

$$\begin{aligned} r_1 &= 0.1(3cos^2\phi - 1)^2 \\ r_2 &= 0.3sin^2(2\phi) \\ r_3 &= 0.3sin^4(\phi) \end{aligned} \tag{10}$$

In the case of a mixture of spherical rotating species, e.g., with rotational correlation times of τ_{corr1} and τ_{corr2}:

$$r(t) = r_1 e^{\left(\frac{-t}{\tau_{corr1}}\right)} + r_2 e^{\left(\frac{-t}{\tau_{corr2}}\right)} \tag{11}$$

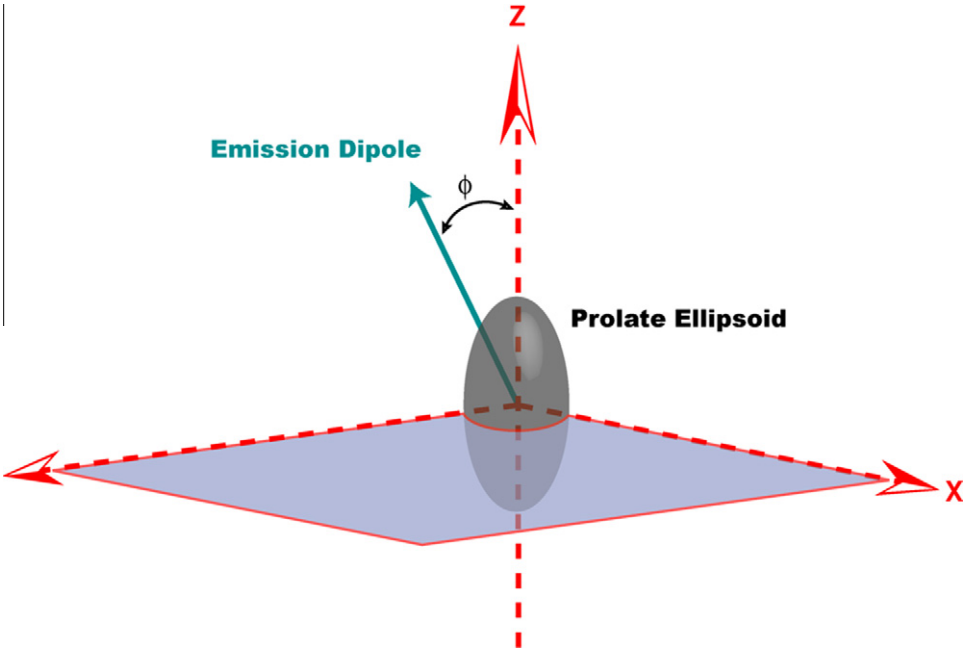

Fig. 8. Depiction of the axes of a prolate ellipsoid of revolution with an emission dipole oriented at an angle to the long axis.

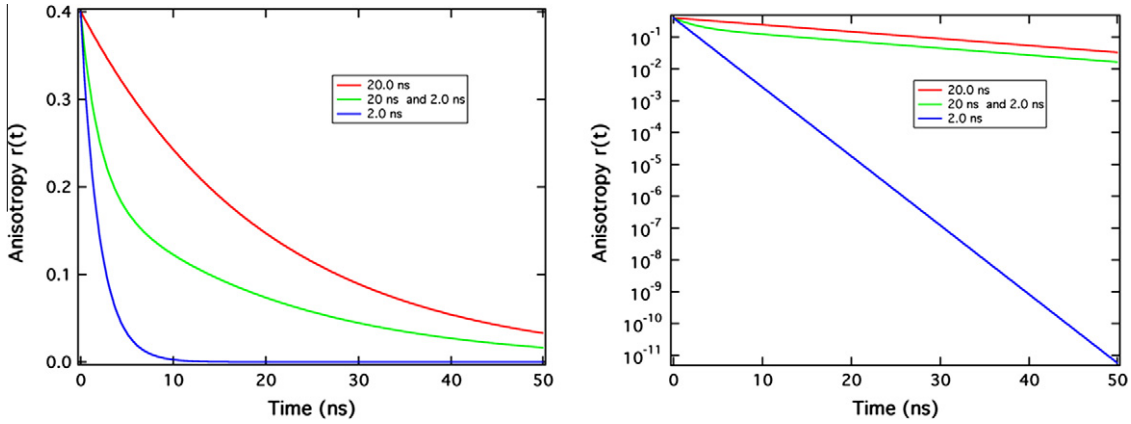

Fig. 9. Depiction of the decay of anisotropies, shown in both linear and logarithmic scales, for two different rotating spheres and a 50:50 mixture. The lifetime of the fluorophores was 20 ns in all cases.

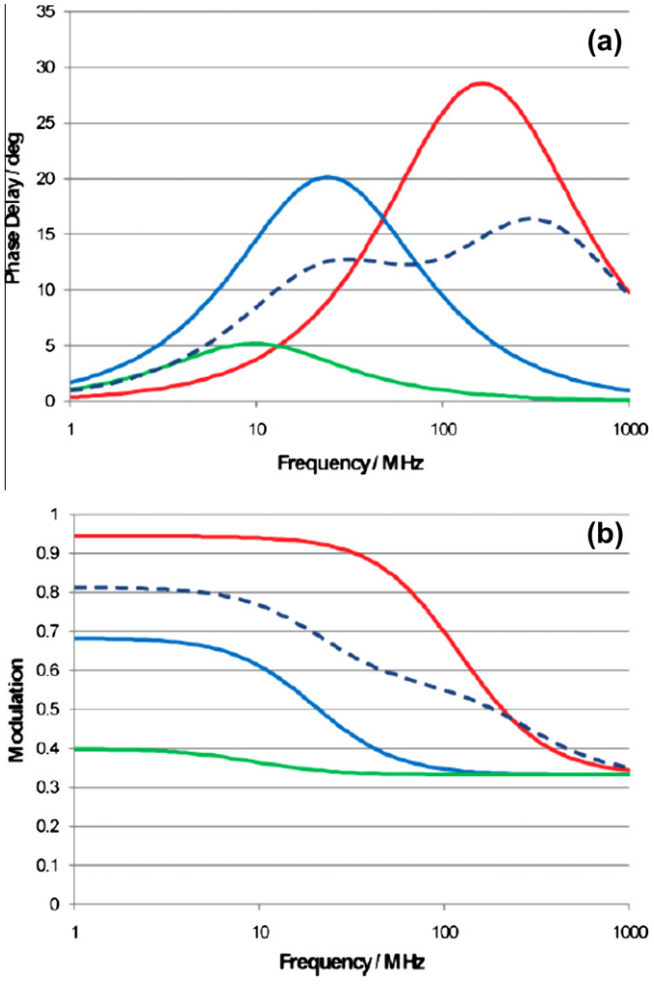

Fig. 10. Differential phase data (a) and modulation ratio (b) for an isotropic rotator with 3 (solid red), 30 (solid blue) and 300 ns (solid green) rotational relaxation times. The dashed blue line in the phase and modulation curves correspond to the case of two rotational relaxation times, namely 30 and 1.5 ns, with associated anisotropies of 0.2 for each component. In each case a fluorescence lifetime of 20 ns was used and colinear excitation and emission dipoles (i.e., limiting anisotropies of 0.4) were assumed.

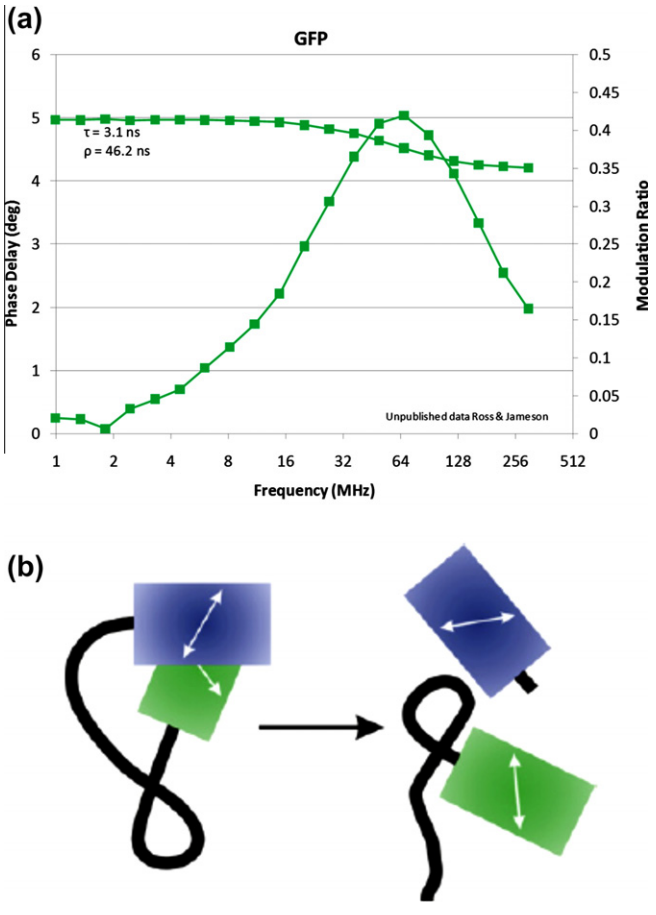

Fig. 11. (a) Dynamic polarization data for GFP in buffer at 22 °C, excited at 471 nm. Unpublished data of Justin A. Ross and David M. Jameson. Both phase delay (bell-shaped curve) and modulation ratio data are shown. (b) Depiction of BFP linked via a short peptide to GFP, before and after cleavage of the linking peptide.

Fig. 9 depicts, with both linear and logarithmic scales, the type of time-decay anisotropy data one would expect for the case of molecules with rotational correlation times of 20 and 2 ns and then a 50:50 mixture of the two molecules (the fluorescence lifetime is taken as 20 ns in each case). Hence one can, in theory, determine how much of each component is present in a mixture of two species, assuming that their rotational correlation times are sufficiently separated.

In the frequency domain equivalent, i.e., dynamic polarization measurements, the sample is illuminated with vertically polarized,

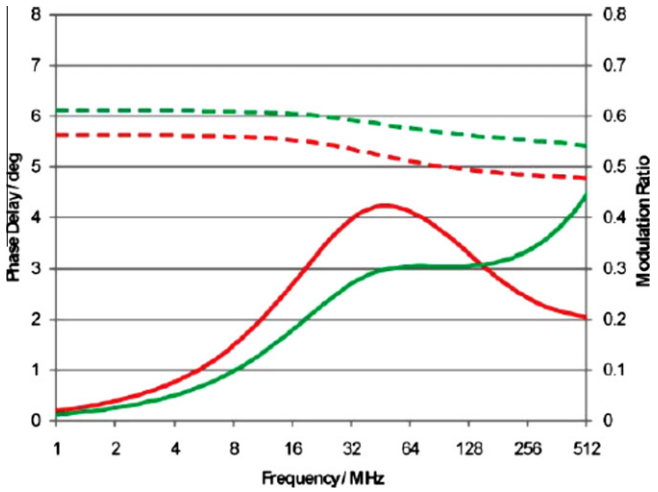

Fig. 12. Differential phase data (solid) and modulation ratio (dashed) EF-Tu-GDP (red) ($t1$ = 4.8 ns, $t2$ = 0.31 ns, $f1$ = 0.79, $r1$ = 63 ns, $r1$ = 0.23, $r2$ = 1.5 ns, $r2$ = 0.05) and EF-Tu-EF-Ts (green) ($t1$ = 4.6 ns, $t2$ = 0.23 ns, $f1$ = 0.82, $r1$ = 84 ns, $r1$ = 0.19, $r2$ = 0.3 ns, $r2$ = 0.12). Adapted from reference 31.

modulated light. The phase delay between the parallel and perpendicular components of the emission is measured as well as the modulation ratio of the AC contributions of these components [28]. The expressions for a spherical particle are [28]:

$$\Delta\phi = \tan^{-1}\left[\frac{3\omega r_o R}{(k^2+\omega^2)(1+r_o-2r_o^2)+6R(6R+2R+kr_o)}\right] \quad (12)$$

$$Y^2 = \frac{[(1-r_o)k+6R]^2+(1+r_o)^2\omega^2}{[(1+2r_o)k+6R]^2+(1+2r_o)^2\omega^2} \quad (13)$$

where $\Delta\phi$ is the phase difference, Y the modulation ratio of the AC components, ω the angular modulation frequency, r_o the limiting anisotropy, k the radiative rate constant $(1/\tau)$ and R the rotational diffusion coefficient. Fig. 10 depicts the $\Delta\phi$ function for the cases of spherical particles with different rotational relaxation times. Fig. 11A shows dynamic polarization data for GFP in aqueous buffer; the data fit well to one Debye rotational relaxation time of 46 ns which is to be expected for a spherical protein of ~25 kDa. Fig. 11B depicts a system of two fluorescent proteins (BFP and GFP) linked by a short peptide which acts as a substrate for the botulinum neurotoxin A protease. The emission of the GFP moiety was isolated with appropriate excitation and emission conditions (details in ref [30]) and the rotational relaxation time of the GFP was measured, using dynamic polarization, before and after cleavage of the peptide and subsequent separation of the BFP and GFP moieties. Rotational relaxation times of ~92 and ~53 ns were found, respectively, for the case of the dimeric protein and GFP alone. The increases in the rotational relaxation time for the GFP cleaved from the substrate compared to free GFP is due to the additional mass of the cleaved peptide. We note that even though the lifetimes in these systems are relatively short (3.1 ns) compared to the rotational relaxation times, accurate determinations are possible in large part due to the absence of local probe mobility. Addition of additional rotational modalities will necessarily complicate the resolution of the rotational rates.

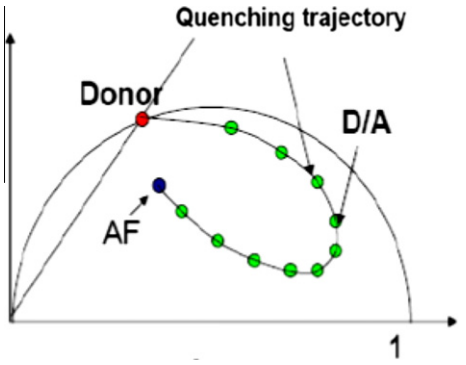

Fig. 14. Depiction of a phasor plot illustrating the position of the phasor point corresponding to a donor along with the phasor point corresponding to cell autofluorescence. As the donor is quenched via FRET the trajectory of the phasor point moves in a specific manner towards the autofluorescence point.

In the case of local plus global motion, the dynamic polarization curves are altered as illustrated in Fig. 12 for the case of the single tryptophan residue in elongation factor Tu (EF-Tu), which shows a dramatic increase in its local mobility when EF-Tu is complexed with elongation factor Ts (EF-Ts) (which has no tryptophan residues) [2,31]. These dynamic polarization data can be analyzed in terms of two rotational relaxation times, namely a slow one of 63 ns and a faster one of 1.5 ns. The slower value was attributed to the "global" motion of the entire protein while the faster value was attributed to the "local" mobility of the tryptophan residue. The contributions to the total anisotropy of these two motions were 0.23 and 0.05, respectively. When the TuTs complex is formed, the "global" rotational relaxation time increased to 84 ns, which is reasonable since the size of the protein complex increased to 77 kDa compared to 43 kDa for EF-Tu alone. The "local" motion in the case of TuTs was 0.3 ns and the contributions to the total anisotropy of the global and local motions were 0.19 and 0.12 in this case. Clearly, binding of Ts led to significantly enhanced local motion of the tryptophan residue, resulting from a large conformational change on the EF-Tu protein matrix. Details of this analysis can be found in the original reference [31].

4. FLIM/FRET and *in vivo* phasors

As mentioned earlier, in recent years the phasor approach has been applied by several groups to FLIM studies. When used in

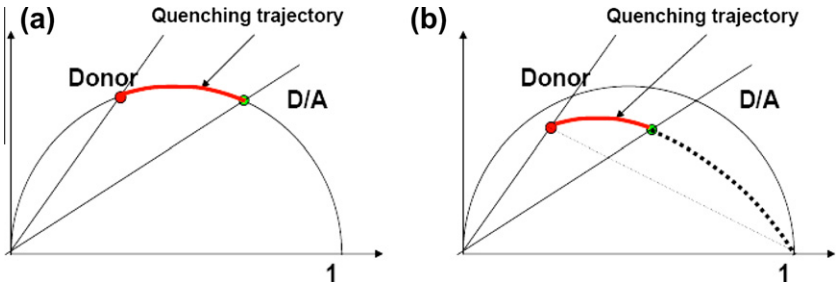

Fig. 13. Depiction of phasor plots illustrating position of the phasor point corresponding to donor alone, for the case of single exponential donor lifetime (a) and in the case of a donor exhibiting a multi-exponential decay (b). In both cases the effect of donor quenching, via FRET, is illustrated to show the trajectory of the phasor point.

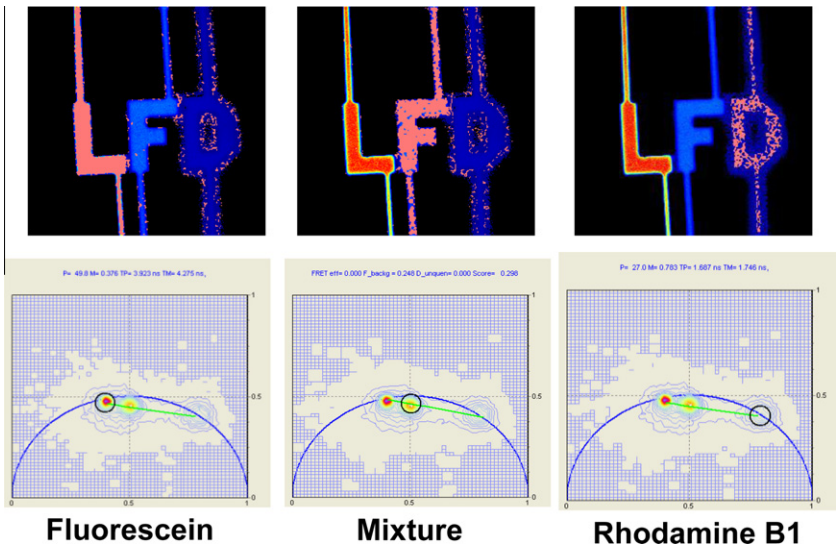

Fig. 15. Illustration of the phasor plot program in the simFCS package (www.lfd.uci.edu). The three letters (L,F,D) are filled with fluorescein (L), rhodamine (D) and a mixture of the two dyes (F). The phasor plots corresponding to the overall image are shown beneath each letter. As the cursor is placed over the different phasor points different letters light up demonstrating which pixels contained the chosen lifetime data.

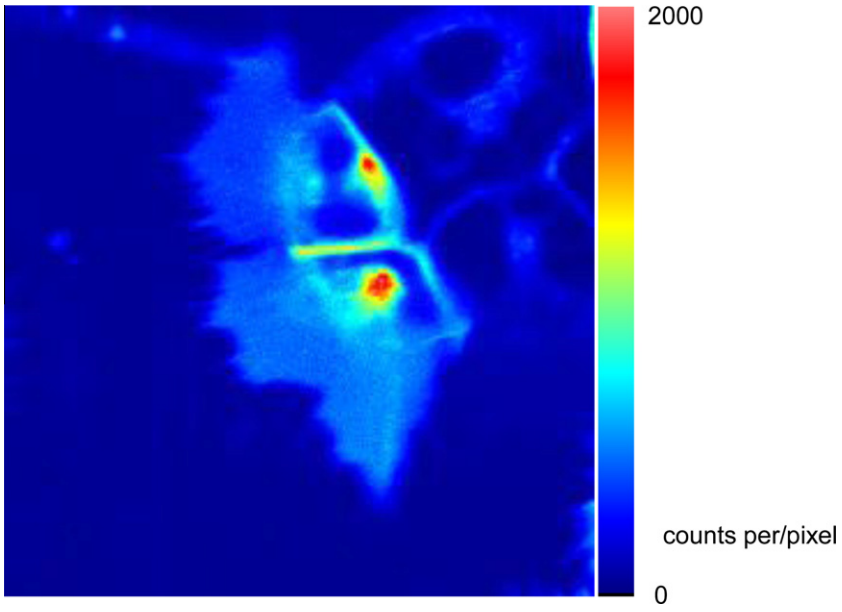

Fig. 16. Intensity image of a cell expressing two different variants of the GPI-anchored urokinase plasminogen activator receptor (from 32).

conjunction with FLIM, the phasor method provides important information on the spatial distribution of lifetime data in images. More importantly, it allows one to discern lifetime-related processes, such as FRET, without recourse to direct analysis of complex decays. In FLIM, lifetime data is obtained at every pixel in the image. Such information can be very useful since the lifetime is not dependent on the number of fluorophores in a particular volume element of the cell, but rather reports on excited state processes in that volume element. In the case of FRET systems, the lifetime of the donor molecule will be reduced by the FRET process and the existence of FRET can be directly ascertained by the decrease in the donor fluorophore's lifetime [7]. Hence, if one protein is labeled with a fluorescent donor while another is labeled with an appropriate acceptor, FRET between the donor and acceptor is unequivocal proof that a protein complex was formed. Of course one difficulty with these types of FRET studies is that the absence of a FRET signal does not prove that the protein complex did not form, since the donor and acceptor dipoles may be too far apart or they may not be oriented properly for FRET to occur [7]. In the case of FLIM on live cell systems, the situation is complicated by the fact that any particular pixel composing the image will not typically have more than 500–1000 photons contributing to the signal. Hence, extracting a precise lifetime is problematic, especially if multiple lifetime components are present. Also, one must often contend with autofluorescence of the cell which makes it very difficult to carry out a rigorous analysis of a donor lifetime. The phasor approach, however, can circumvent this difficulty since in "phasor space" as the donor lifetime is quenched via FRET the phasor point will move along a predictable trajectory towards the cell autofluorescence. The principles underlying the application of

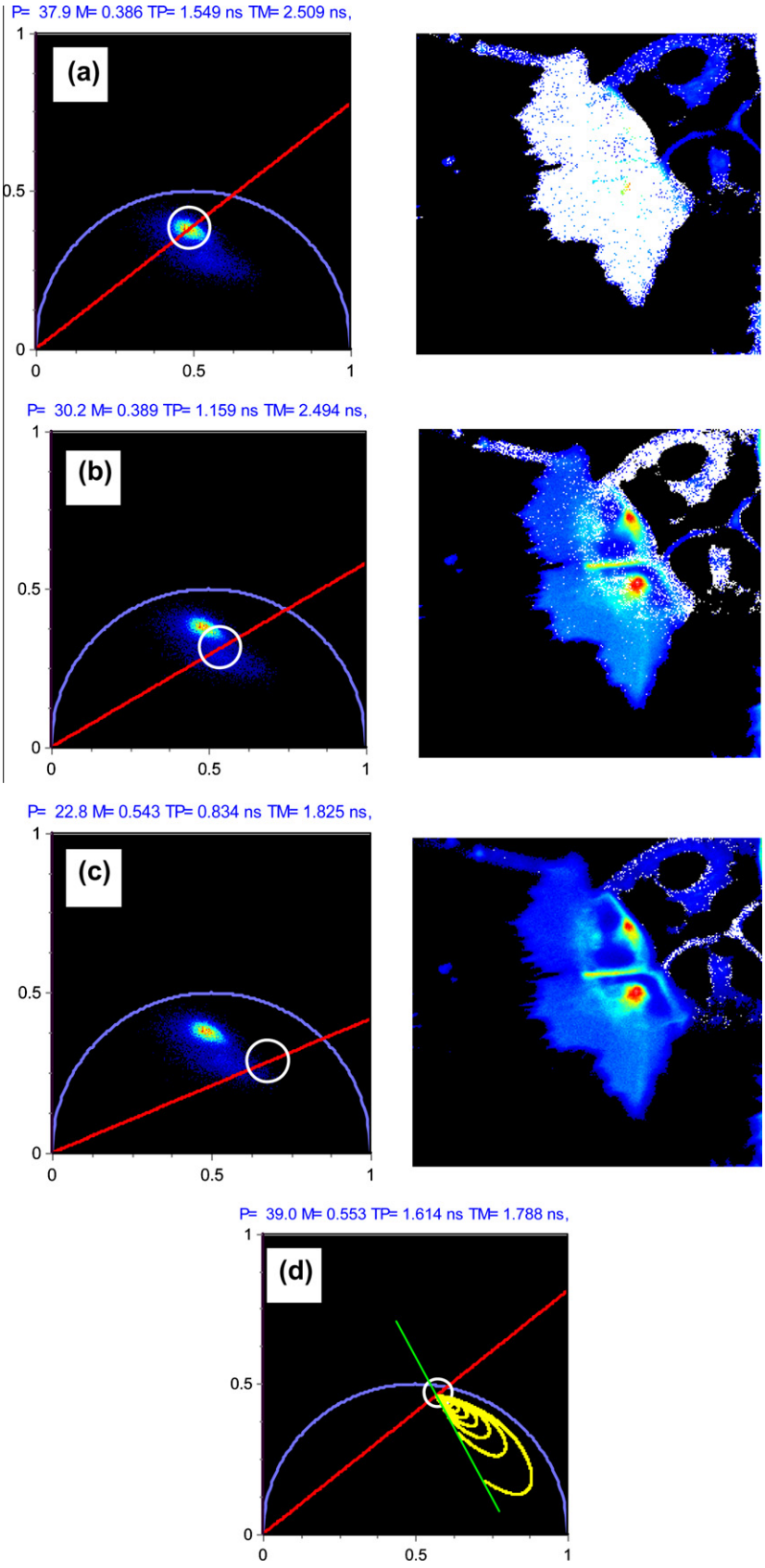

Fig. 17. Selecting regions of the phasor diagram. Selecting the region in (a) (donor + acceptor) the part in white lights up. Selecting the region in (b) (autofluorescence) the part in white in lights up. The color scale has been changed to better show the region of the autofluorescence. Selecting the region in (c′) (along the donor quenching line as shown in (d)) the part in white in at the cell junction lights up in (c).

phasors to FRET processes in FLIM images are illustrated in Figs. 13 and 14. Fig. 13 shows the trajectory a phasor point will take along the universal circle when the donor lifetime is single exponential decay (A) and when the donor lifetime is a more complex, multi-exponential decay (B). Fig. 14 depicts the case of a multi-exponential decay but with the addition of autofluorescence. One notes that as the FRET efficiency increases and the phasor point moves its trajectory curves back towards the phasor due to the autofluorescence signal. Using the FLIM analysis software in the Globals for Images software package, developed by Enrico Gratton and available from the Laboratory for Fluorescence Dynamics (www.LFD.UCI.edu), one can put a cursor on any point in the phasor diagram and the pixels corresponding to those phasor values will be illuminated. This principle is illustrated in Fig. 15. Microchannels in the shape of the letters L, F and D (which stand for the Laboratory for Fluorescence Dynamics) were filled with either fluorescein (L), rhodamine B1 (D) or a mixture of these two dyes. The phasor diagram corresponding to the image are shown in the bottom row of the Fig. 15. When the cursor is placed over the phasor region on the left side of the plot, the pixels corresponding to those phasor points, in this case due to fluorescein, are illuminated (in pink in this image). Correspondingly when the cursor is placed over the phasor points due to rhodamine, the pixels in the letter D are illuminated. Finally, when the cursor is placed over the points corresponding to the mixture, the pixels in the letter F are highlighted. This example nicely illustrates how FLIM images can be interrogated using the phasor diagram. The images in Figs. 16 and 17 were from a study by Caiolfa et al. [32] on the oligomerization state of the GPI-anchored urokinase plasminogen activator receptor (uPAR). Fig. 16 shows the two-photon intensity image of HEK293 cells transfected with GFP and RFP constructs of uPAR. If the uPAR dimerizes one expects to detect FRET between the EFGP and RFP moieties and hence a lower lifetime for the EGFP-uPAR. In the case of monomeric EGFP-uPAR, however, the EGFP lifetime should be unquenched. Fig. 17 shows the phasor plots corresponding to the FLIM image and illustrates how different regions of the cells are highlighted as the cursor is placed on different regions of the phasor plot. One can clearly distinguish between unquenched EGFP region (A), the pixels contributing mainly to autofluorescence (B) and the regions – where cells are in contact – showing quenched EGFP due to FRET (C). Panel D illustrates different possible FRET quenching trajectories showing how they are off the main line connecting the donor fluorescence with the autofluorescence. Hence one can easily demonstrate where in the cell images the uPAR protein can dimerize.

5. Closing remarks

Hopefully, in this short review we have illustrated how time-resolved fluorescence – and in particular phasors – can be used to study protein interactions both in and out of cells. This field is still relatively new and novel applications of the phasor approach are appearing regularly. The availability of software packages, such a Globals for Images, from the Laboratory for Fluorescence Dynamics, is helping to drive progress in this field. Companies which provide instruments designed for time-resolved cuvette studies are also starting to provide phasor routines in their software packages, e.g., ISS, Inc with its Vista software. We suggest that anyone interesting in time-resolved studies on complex systems consider the phasor approach.

Acknowledgments

We wish to thank Dr. Theodore Hazlett for drawing several of the figures used in this article. We also thank Dr. Enrico Gratton for several of the figures related to phasors and FLIM. We acknowledge financial support from Allergan, Inc.

References

[1] D.M. Jameson, in: B. Valeur, J.-C. Brochon (Eds.), New Trends in Fluorescence Spectroscopy, Springer, Verlag, Berlin, 2001, pp. 35–58.
[2] J.A. Ross, D.M. Jameson, J. Photochem. Photobiol. Sci. 7 (2008) 1301–1312.
[3] G.T. Hermanson, Bioconjugate Techniques, Academic Press, San Diego, California, 1996.
[4] S.S. Wong, D.M. Jameson, Chemistry of Protein and Nucleic Acid Cross-Linking and Conjugation, Taylor and Francis, New York, N.Y., 2012.
[5] D.M. Jameson, N.G. James, J.P. Albanesi, Meth. Enzymol. 519 (2013) 87–113.
[6] D.M. Jameson, J.A. Ross, Rev. Fluoresc. Polarization/Anisotropy Clin. Diagnostics Imaging 110 (2010) 2685–2708.
[7] B. Valuer, M.N. Berberan-Santos, Molecular fluorescence principles and applications, second ed., Wiley, VCN-Weiheim (Germany), 2012.
[8] C.D. McGuinness, K. Sagoo, D. McLoskey, D.J.S. Birch, Meas. Sci. Technol. 15 (2004) 19–22.
[9] E. Gaviola, Ann. Phys. 386 (1926) 681–710.
[10] R.D. Spencer, G. Weber, Ann. N. Y. Acad. Sci. 158 (1969) 361–376.
[11] E. Gratton, M. Limkeman, Biophys. J. 44 (1983) 315–324.
[12] B. Barbieri, E. Terpetschnig, D.M. Jameson, Anal. Biochem. 344 (2005) 298–300.
[13] E. Gratton, D.M. Jameson, N. Rosato, G. Weber, Rev. Sci. Instrum. 55 (1984) 486–494.
[14] J.R. Alcala, E. Gratton, D.M. Jameson, Anal. Instrum. 14 (1985) 225–250.
[15] D.M. Jameson, E. Gratton, R.D. Hall, Appl. Spectrosc. Rev. 20 (1984).
[16] R. Alcala, E. Gratton, F.G. Prendergast, Biophys. J. 51 (1987) 587–596.
[17] J.C. Brochon, Methods Enzymol. 240 (1994) 262–311.
[18] F. Dushinsky, Z. Phys. A 81 (1933) 7–22.
[19] G. Weber, J. Phys. Chem. 85 (1981) 949–953.
[20] M. Stefl, N.G. James, J.A. Ross, D.M. Jameson, Anal. Biochem. 410 (2011) 62–69.
[21] G.D. Reinhart, P. Marzola, D.M. Jameson, E. Gratton, J. Fluoresc. 1 (1992) 153–162.
[22] K.M. Hirshfield, D. Toptygin, B.S. Packard, L. Brand, Anal Biochem. 209 (1993) 209–218.
[23] M.A. Digman, V.R. Caiolfa, M. Zamai, E. Gratton, Biophys. J. 94 (2008) 14–16.
[24] Q.S. Hanley, A.H.A. Clayton, J. Microsc. 218 (2005) 62–67.
[25] G.I. Redford, R.M. Clegg, J. Fluoresc. 15 (2005) 805–815.
[26] N.G. James, J.A. Ross, M. Stefl, D.M. Jameson, Anal. Biochem. 410 (2011) 70–76.
[27] R. Buscaglia, D.M. Jameson, J.B. Chaires, Nucleic Acids Res. 40 (2012) 4203–4215.
[28] E. Gratton, D.M. Jameson, R.D. Hall, Ann. Rev. Biophys. 13 (1984) 105–124.
[29] D.M. Jameson, T.L. Hazlett, in: G. Dewey (Ed.), Biophysical and Biochemical Aspects of Fluorescence Spectroscopy, Plenum Press, N.Y., 1991, pp. 105–133.
[30] J.A. Ross, M.A. Gilmore, D. Williams, K.R. Aoki, L.E. Steward, D.M. Jameson, Anal. Biochem. 413 (2011) 43–49.
[31] D.M. Jameson, E. Gratton, J.F. Eccleston, Biochemistry 26 (1987) 3894–3901.
[32] V.R. Caiolfa, M. Zamai, G. Malengo, A. Andolfo, C.D. Madsen, J. Sutin, M.A. Digman, E. Gratton, F. Blasi, N. Sidenius, J. Cell Biol. 179 (2007) 1067–1082.